

GENERALIZED FINITE ELEMENT METHOD ON HYBRID STRESS APPROACH: FORMULATION AND NUMERICAL PERFORMANCE

Wesley Góis^a, Sergio P. B. Proença^b

^a*Aerospace Engineering, Center of Engineering, Modeling, and Applied Social Sciences, Federal University of ABC, Santa Adélia Street 166, CEP 09210-170, Santo André, Brazil,
wesley.gois@ufabc.edu.br, <http://www.ufabc.edu.br/>*

^b*Structural Engineering Department, School of Engineering at São Carlos, University of São Paulo,
São-carlense Avenue 400, CEP 13566-590 São Carlos, Brazil, persival@sc.usp.br,
<http://www.set.eesc.usp.br/>*

Keywords: Generalized Finite Element Method, Hybrid Stress Formulation, Element Distortion Sensitivity.

Abstract. The framework of the Generalized Finite Element Method (GFEM) is applied to a nonconventional Hybrid Stress Formulation (HSF) aiming linear plane analysis. In the original HSF two approximation fields are involved: stresses in the domain and displacements on the static boundary. The main features of the HSF are that the stress field satisfies equilibrium condition in the domain, while equilibrium on the common boundaries between elements is enforced in a weak form. In the combined GFEM-HSF approach the enrichment of the displacement boundary field is provided by the product of the partition of unity (PU) and a basis of polynomials enrichment functions. Quadrilateral and triangular finite elements with selective nodal enrichment are then derived. The numerical performance of the HSF with nodal enrichment formulation is tested in several examples. The numerical investigation focuses mainly a sensitivity analysis of the results to mesh distortion. Relating to this aspect some mesh distortion conditions imposed over plane stress beam-bending benchmarks are addressed. In addition, considering both computational and numerical aspects, one conclude that GFEM-HSF can provide good alternative to conventional displacement based formulations for plane linear analysis.

1 INTRODUCTION

This work addresses some recent developments on the nonconventional finite elements formulation for linear plane analysis derived from a Hybrid Stress Formulation (HSF) with nodal enrichment, Góis and Proença (2007a,b) and Góis (2009a).

In the original HSF proposed in Freitas, Almeida e Pereira (1996) two independent approximation fields are involved: stresses in the domain and a displacement field on the static boundary, i.e., part of the boundary where surface forces are imposed. Due to this particular feature such nonconventional formulation is typified as Hybrid. An additional basic feature of the HSF here adopted is that equilibrium through common boundaries between elements is weakly imposed, once the discretized domain is considered. In view of this fact, the non-conventional form is finally referenced as a Hybrid Stress Formulation (HSF).

On the other hand, the Generalized Finite Element Method (GFEM), originally presented in Oden, Duarte and Zienkiewicz (1998), is essentially a partition of unity (PU) based approach involving a nodal enrichment strategy. The enrichment feature consists on a p-refinement of the approximation fields, however without introducing additional nodes over an adopted discretization mesh, Duarte and Oden (1995). Therefore, the nodal strategy differs from the finite element p-adaptive classical process.

In this work both HSF and a nodal enrichment strategy of the boundary displacement field are combined generating a new class of finite elements for linear plane analysis. One particular feature of this class of elements is its insensitivity to mesh distortion. In order to emphasize such aspect, distortion sensitivity tests are conducted considering four nodes quadrilateral HSF elements.

On the other hand, considering the independence of the approximation fields provided to the displacement on the boundary and the stresses in the domain, the enrichment could be unconditionally imposed to the boundary displacement field. However, such an option is restricted by stability aspects. Actually, in this study a kind of inspection test controlling the balance between the number of related stresses and displacement variables is adopted in order supply stable and convergent solutions.

On what follows, in section 2 the HSF for plane elasticity is addressed. The section 3 is devoted to the GFEM formulation in the HSF. In section 4 some numerical experiments related to the distortion sensitivity are presented. Finally, in section 5 the conclusions of the present study are given.

2 HYBRID STRESS FORMULATION (HSF) IN PLANE ELASTICITY

Based on Freitas, Almeida e Pereira (1996), considering a linear-elastic solid of domain Ω and boundary Γ composed by complementary parts Γ_u and Γ_t , where kinematic and static boundary conditions are imposed, respectively, the following Galerkin weighting relations for the compatibility and equilibrium conditions can be written:

$$\int_{\Omega} \delta\sigma^T (L^T u - f\sigma) d\Omega = 0. \quad (1)$$

$$\int_{\Omega} \delta u^T (L\sigma + b) d\Omega = 0. \quad (2)$$

$$\int_{\Gamma_t} \delta u_{\Gamma_t}^T (\bar{t} - N\sigma) d\Gamma = 0. \quad (3)$$

In Eq. (1), Eq. (2) and Eq. (3) the following domain fields are involved: stresses σ , strains

ε and displacements u . In particular, the first relation includes the constitutive condition as well. In addition L is the divergence operator; b the vector of body forces; N the matrix formed by the components of the unit vector normal to the boundary Γ ; f the flexibility matrix for isotropic linear elastic material and \bar{t} the vector of applied superficial forces on Γ_t .

Assuming that the kinematic restriction $\bar{u} = 0$ is strongly imposed on Γ_u and considering Eq. (1) transformed by the Divergence Theorem one obtains:

$$\int_{\Omega} \delta\sigma^T f \sigma d\Omega + \int_{\Omega} (L\delta\sigma)^T u d\Omega - \int_{\Gamma} (N\delta\sigma)^T u d\Gamma = 0. \quad (4)$$

Once a finite element mesh is adopted the boundary Γ for hybrid formulation includes the common inner boundary between elements defined as Γ_i . Therefore, by definition: $\Gamma = \Gamma_i + \Gamma_t + \Gamma_u$ and Eq. (4) takes the following form:

$$\int_{\Omega} \delta\sigma^T f \sigma d\Omega + \int_{\Omega} (L\delta\sigma)^T u d\Omega - \int_{\Gamma_i} (N\delta\sigma)^T u_{\Gamma_i} d\Gamma - \int_{\Gamma_i} (N\delta\sigma)^T u_{\Gamma_i} d\Gamma = 0. \quad (5)$$

Here, displacement continuity between elements on Γ_i is strongly imposed, implying that this part of the boundary can be assumed as a Neumann boundary where equilibrium is verified in a weak form. Then, considering that there are no superficial forces \bar{t} prescribed on Γ_i , the correspondent weak equilibrium relation $\int_{\Gamma_i} \delta u_{\Gamma_i}^T (N\sigma) d\Gamma$ is added to the Eq. (3) and this equation can be expressed as:

$$\int_{\Gamma_i} \delta u_{\Gamma_i}^T (N\sigma) d\Gamma + \int_{\Gamma_i} \delta u_{\Gamma_i}^T (N\sigma) d\Gamma - \int_{\Gamma_i} \delta u_{\Gamma_i}^T (\bar{t}) d\Gamma = 0. \quad (6)$$

Actually, Eq. (2), Eq. (5) and Eq. (6) correspond to a more general Hybrid-Mixed Stress Formulation (HMSF) typified by three independent fields: stresses and displacements defined in the domain Ω and displacements defined on the boundary. In such a general framework it is assumed that the displacements on the boundary Γ_u are prescribed with zero value.

The following approximations for the independent fields could then be introduced:

$$\tilde{\sigma} = S_{\Omega} s_{\Omega}. \quad (7)$$

$$\tilde{u} = U_{\Omega} q_{\Omega}. \quad (8)$$

$$\tilde{u}_{\Gamma_i} = U_{\Gamma_i} q_{\Gamma_i}. \quad (9)$$

$$\tilde{u}_{\Gamma_i} = U_{\Gamma_i} q_{\Gamma_i}. \quad (10)$$

In the preceding relations, s_{Ω} represents the vector of nodal stress variables, while q_{Ω} , q_{Γ_i} and q_{Γ_i} are vectors of nodal degrees of freedom related to the displacements. Furthermore, S_{Ω} , U_{Ω} , U_{Γ_i} and U_{Γ_i} are respectively the matrices collecting the approximation functions for stress and displacement fields.

Applying the approximations given by Eq. (7) to Eq. (10) in Eq. (2), Eq. (5) and Eq. (6), the following linear system of equations governing the HMSF could be deduced:

$$\begin{bmatrix} F & A_{\Omega} & -A_{\Gamma_t} & -A_{\Gamma_i} \\ A_{\Omega}^T & 0 & 0 & 0 \\ -A_{\Gamma_t}^T & 0 & 0 & 0 \\ -A_{\Gamma_i}^T & 0 & 0 & 0 \end{bmatrix} \begin{Bmatrix} s_{\Omega} \\ q_{\Omega} \\ q_{\Gamma_t} \\ q_{\Gamma_i} \end{Bmatrix} = \begin{Bmatrix} 0 \\ -Q_{\Omega} \\ -Q_{\Gamma_t} \\ 0 \end{Bmatrix}. \quad (11)$$

In Eq. (11) the following matrices were introduced:

$$F = \int_{\Omega} S_{\Omega}^T f S_{\Omega} d\Omega. \quad (12)$$

$$A_{\Omega} = \int_{\Omega} (LS_{\Omega})^T U_{\Omega} d\Omega. \quad (13)$$

$$A_{\Gamma_t} = \int_{\Gamma_t} (NS_{\Omega})^T U_{\Gamma_t} d\Gamma. \quad (14)$$

$$A_{\Gamma_i} = \int_{\Gamma_i} (NS_{\Omega})^T U_{\Gamma_i} d\Gamma. \quad (15)$$

$$Q_{\Omega} = \int_{\Omega} U_{\Omega}^T b d\Omega. \quad (16)$$

$$Q_{\Gamma_t} = \int_{\Gamma_t} U_{\Gamma_t}^T \bar{t} d\Gamma. \quad (17)$$

The reason to present the general framework of the HSMF is that HSF can then be derived from it assuming that the stress approximations locally satisfy the equilibrium condition. Moreover, if no body forces are considered the stress approximations compose a self-equilibrated field, thus satisfying:

$$LS_{\Omega} = 0. \quad (18)$$

Once this condition is assumed, the matrices A_{Ω} and Q_{Ω} vanish and Eq. (11) simplifies to:

$$\begin{bmatrix} F & -A_{\Gamma_t} & -A_{\Gamma_i} \\ -A_{\Gamma_t} & 0 & 0 \\ -A_{\Gamma_i} & 0 & 0 \end{bmatrix} \begin{Bmatrix} s_{\Omega} \\ q_{\Gamma_t} \\ q_{\Gamma_i} \end{Bmatrix} = \begin{Bmatrix} 0 \\ -Q_{\Gamma_t} \\ 0 \end{Bmatrix}. \quad (19)$$

Accordingly, no displacement fields in the domain are involved in the HSF approach.

3 FINITE ELEMENT APPROACH AND NODAL ENRICHMENT IN HSF

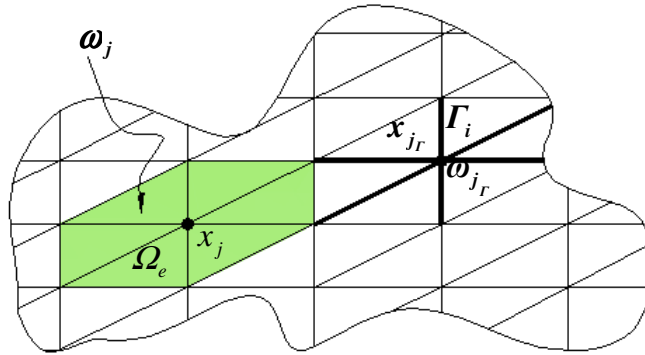


Figure 1: Domain and boundary elements

The element meshes employed for discretizing domain and boundary regions are indicated [Figure 1](#). Either four-node quadrilateral elements (see [Figure 2](#)) or three-node triangular (see [Figure 3](#)) elements can be used in the domain discretization. On the boundary regions classical linear elements are defined.

The geometry of the quadrilateral element (see [Figure 2](#)) is built from a master element using the conventional Lagrangian bilinear functions indicated in Eq. (20) to Eq (23).

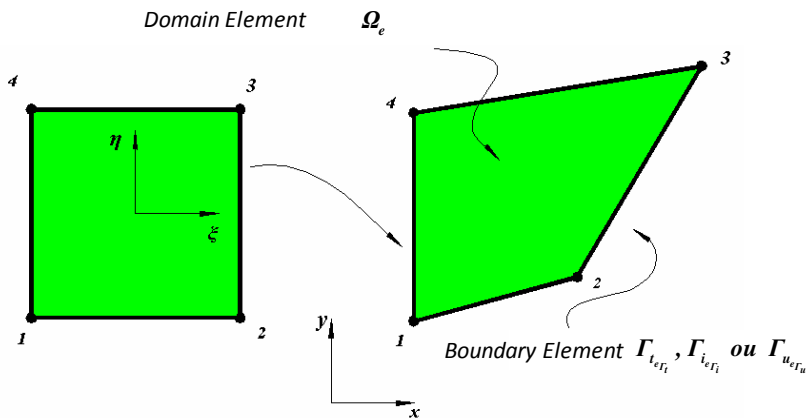


Figure 2: Four-node quadrilateral element

$$\varphi_1(\xi, \eta) = \frac{1}{4}(\xi - 1)(\eta - 1). \quad (20)$$

$$\varphi_2(\xi, \eta) = -\frac{1}{4}(\xi + 1)(\eta - 1). \quad (21)$$

$$\varphi_3(\xi, \eta) = \frac{1}{4}(\xi + 1)(\eta + 1). \quad (22)$$

$$\varphi_4(\xi, \eta) = -\frac{1}{4}(\xi - 1)(\eta + 1). \quad (23)$$

In the relations above ξ and η are the dimensionless coordinates taking values from -1 to 1.

The typical triangular element employed is depicted in [Figure 3](#). The normalized triangular coordinates are defined by Eq. (24) to Eq. (26).

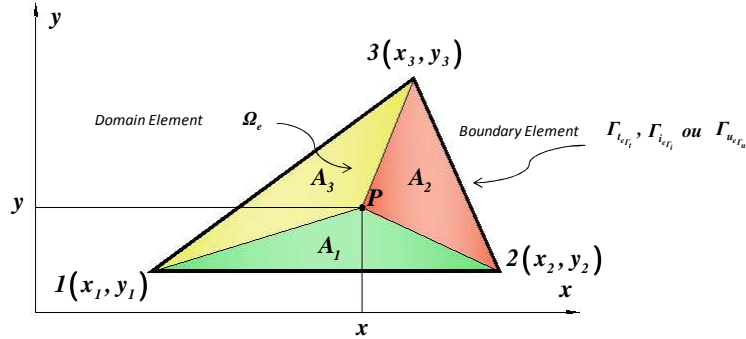


Figure 3: Three-node triangular element

$$\xi_1 = \frac{A_1}{A_e}. \quad (24)$$

$$\xi_2 = \frac{A_2}{A_e}. \quad (25)$$

$$\xi_3 = \frac{A_3}{A_e}. \quad (26)$$

where A_1, A_2 and A_3 are the areas indicated in [Figure 3](#) and A_e is for the total area of the triangle.

The linear Lagrangian linear functions of the boundary elements attached to the quadrilateral elements sides are defined in local coordinates as:

$$\psi_1 = -\frac{I}{2}(\xi - 1). \quad (27)$$

$$\psi_2 = \frac{I}{2}(\xi + 1). \quad (28)$$

The local coordinate ξ varies from -1 to 1.

While for the boundary elements attached to the triangular elements sides one has:

$$\psi_1 = (1 - \xi). \quad (29)$$

$$\psi_2 = \xi. \quad (30)$$

In this case, the local coordinate ξ varies from 0 to 1.

As already mentioned the HSF stress field approximations are assumed to be self-

equilibrated. In this work polynomial Airy functions ($A(x, y)$) are adopted to accomplish that particular feature. Thus, constant, linear and quadratic element stresses approximations can be defined:

Constant approximation

$$S_{\Omega_e} = \begin{bmatrix} 1 & 0 & 0 \\ 0 & 1 & 0 \\ 0 & 0 & 1 \end{bmatrix}. \quad (31)$$

Linear approximation

$$S_{\Omega_e} = \begin{bmatrix} 1 & 0 & 0 & \vdots & y & -x & 0 & 0 \\ 0 & 1 & 0 & \vdots & 0 & 0 & -y & x \\ 0 & 0 & 1 & \vdots & 0 & y & x & 0 \end{bmatrix}. \quad (32)$$

Quadratic approximation

$$S_{\Omega_e} = \begin{bmatrix} 1 & 0 & 0 & \vdots & y & -x & 0 & 0 & \vdots & y^2 & -2xy & x^2 & 0 & 0 \\ 0 & 1 & 0 & \vdots & 0 & 0 & -y & x & \vdots & 0 & 0 & y^2 & -2xy & x^2 \\ 0 & 0 & 1 & \vdots & 0 & y & x & 0 & \vdots & 0 & y^2 & -2xy & x^2 & 0 \end{bmatrix}. \quad (33)$$

In order to provide enrichment of the boundary approximation field, the boundary cloud concept is introduced. As depicted in [Figure 1](#) a boundary cloud attached to a node is defined by the linear elements sharing that node. The enrichment of the boundary displacement field can then be performed following the PU based approach of the Generalized Finite Element Method (GFEM), [Oden, Duarte and Zienkiewicz \(1998\)](#). In this work, the option for polynomial enrichment is explored.

Thus, assuming that a two-dimensional domain has been meshed with HSF four-node quadrilateral or three-node triangular elements, the following HSF-GFEM boundary shape functions can be indicated:

$$\Xi_{N\Gamma}^I = \left\{ \left\{ U_{\Gamma_{j\Gamma}} \right\}_{j\Gamma=1}^{N_\Gamma} \cup \left\{ U_{\Gamma_{j\Gamma}} h_{j\Gamma n_{e\Gamma}} \right\}_{j\Gamma=1}^{N_\Gamma} : j_\Gamma = 1, \dots, N_\Gamma; n_{e\Gamma} = 1, \dots, I(j_\Gamma) \right\}. \quad (34)$$

The boundary displacement approximation field can then be constructed as:

$$\hat{u}_\Gamma = \sum_{j\Gamma=1}^{N_\Gamma} U_{\Gamma_{j\Gamma}} \left\{ u_{\Gamma_{j\Gamma}} + \sum_{i=1}^{n_{e\Gamma}} h_{j\Gamma i} d_{j\Gamma i} \right\}. \quad (35)$$

where $U_{\Gamma_{j\Gamma}}$ are the displacement approximations (see, Eq. (34)), $u_{\Gamma_{j\Gamma}}$ are the displacement degrees of freedom associated with the original shape functions, $d_{j\Gamma i}$ are the additional nodal parameters introduced by the enrichment, $n_{e\Gamma}$ is for the number of enrichment functions defined in each index node j_Γ . Then, the following matrix notation can be used to indicate the HSF-GFEM shape functions:

$$U_{\Gamma_i} = U_{\Gamma_i} = \begin{bmatrix} \psi_1 \Delta_{\Gamma_i} & \psi_2 \Delta_{\Gamma_i} \end{bmatrix}. \quad (36)$$

In the relation above I_2 represents the identity matrix of second order and $\Delta_{\Gamma_{j_r}}$ is given by:

$$\Delta_{\Gamma_{j_r}} = \begin{bmatrix} I_2 & h_{11}I_2 & \dots & h_{j_r k}I_2 & \dots & h_{j_r n_{e_r}}I_2 \end{bmatrix}. \quad (37)$$

A final remark is that by convenience the enrichment functions $h_{j_r n_{e_r}}$ are adopted in such a way that they are null at the attached nodes, thus not destroying the meaning of the original nodal parameters. Essentially, they are given by:

- x

$$h_{j_r n_{e_r}}(\xi, \eta) = (\psi_1 x_1 + \psi_2 x_2) - x_{j_r}. \quad (38)$$

- y

$$h_{j_r n_{e_r}}(\xi, \eta) = (\psi_1 y_1 + \psi_2 y_2) - y_{j_r}. \quad (39)$$

4 NUMERICAL ANALYSIS

In the whole set of examples hereby presented, the enrichment methodology was performed in such a way that the number of stress variables was always greater than the number of nodal displacement parameters, including the ones introduced by the enrichment. This procedure derives from the Zienkiewicz-patch test extended to HSF with nodal enrichment, [Góis and Proenca \(2007a\)](#), and ensures stability of the numerical results.

As the first example, the HSF approach with nodal enrichment is tested on what concerns to mesh distortion sensitivity. Two quadrilateral elements are employed to discretize the two problems illustrated in [Figure 4](#): a) a cantilever under pure moment applied at its right edge and b) a cantilever subjected to action of a shear force applied at its right edge.

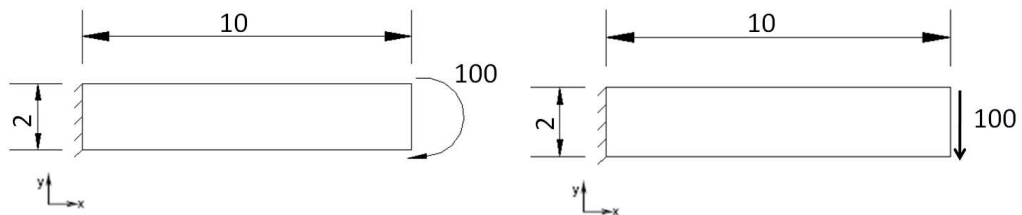


Figure 4: Cantilever beam

As the main purpose here is to analyze the numerical performance of the proposed approach, for convenience no units for the elastic parameters and dimensions are adopted, therefore the following values to the Young's Modulus and Poisson's ratio, respectively, are assumed: $E = 1$ and $\nu = 0.25$.

The cantilever mesh is progressively distorted as depicted in [Figure 5](#). As can be seen, each mesh is typified by the distortion parameter (μ) value. Such a parameter is referenced later in the graphics of the numerical performance. The distortion parameter value was calculated by the rate of the differences between the coordinates x of the two central nodes and the cantilever prescribed length.

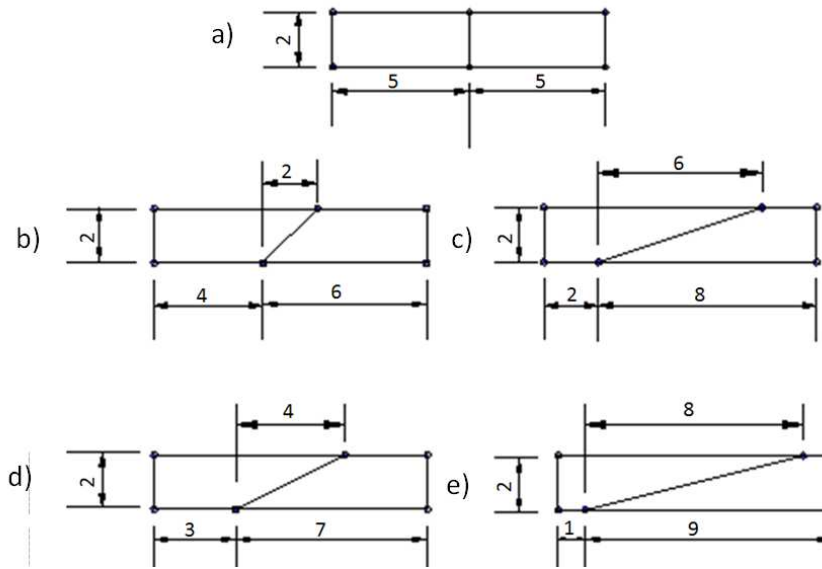


Figure 5: Quadrilateral element meshes

The reference values to both the right side vertical displacement u_y and the strain energy U of problem a) are, respectively: $u_y = -7,500$ and $U = 75,000$; while the references values generated with a very refined mesh for problem b) are: $u_y = -1.03e05$ and $U = 1.03e07$. Concerning the results analysis, both displacement and strain energy were normalized by the reference values.

Regarding problem a), in Figure 6 is shown that considering quadratic stress approach in the domain and without nodal enrichment of the boundary displacement field the HSF quadrilateral element is strongly affected by mesh distortion.

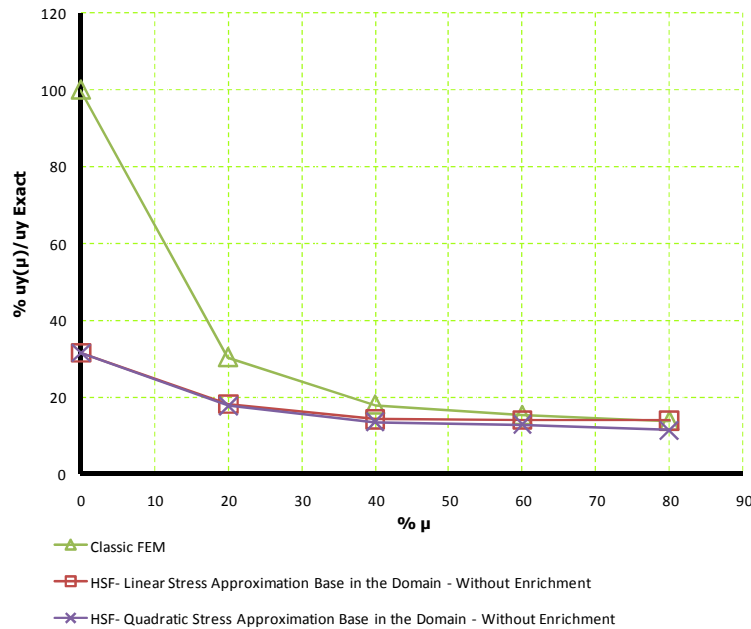


Figure 6: Normalized displacement - quadrilateral element mesh without enrichment

A simple nodal enrichment of the boundary displacement field by means of the function

(x) improves the response of the quadrilateral element HSF with quadratic stress approximation, reducing its sensitivity even in an extreme distortion condition, as shown in [Figure 7](#) and [Figure 8](#). The enrichment was not imposed on the restrained boundary nodes.

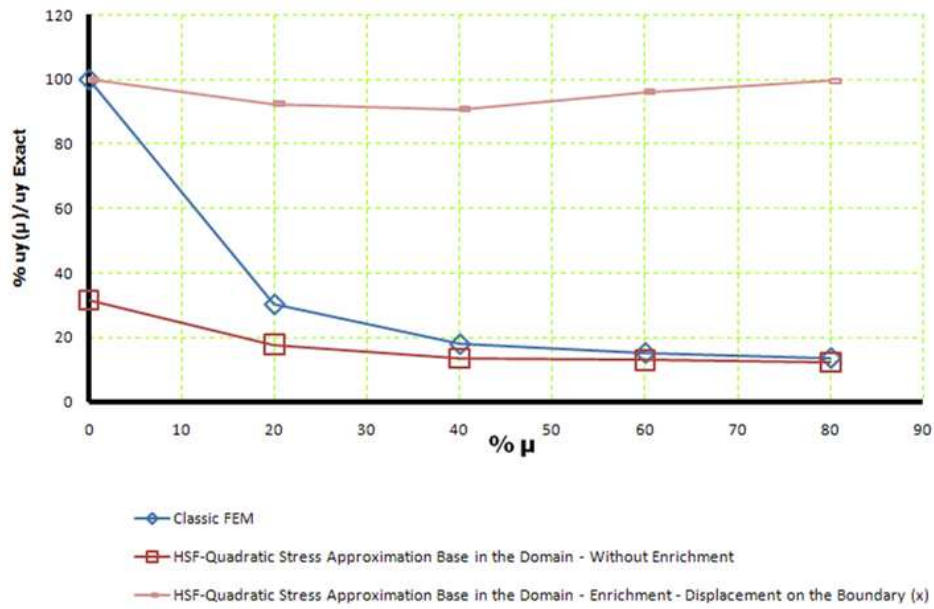


Figure 7: Problem a): displacement - quadrilateral element - enrichment imposed to selective nodes on boundary

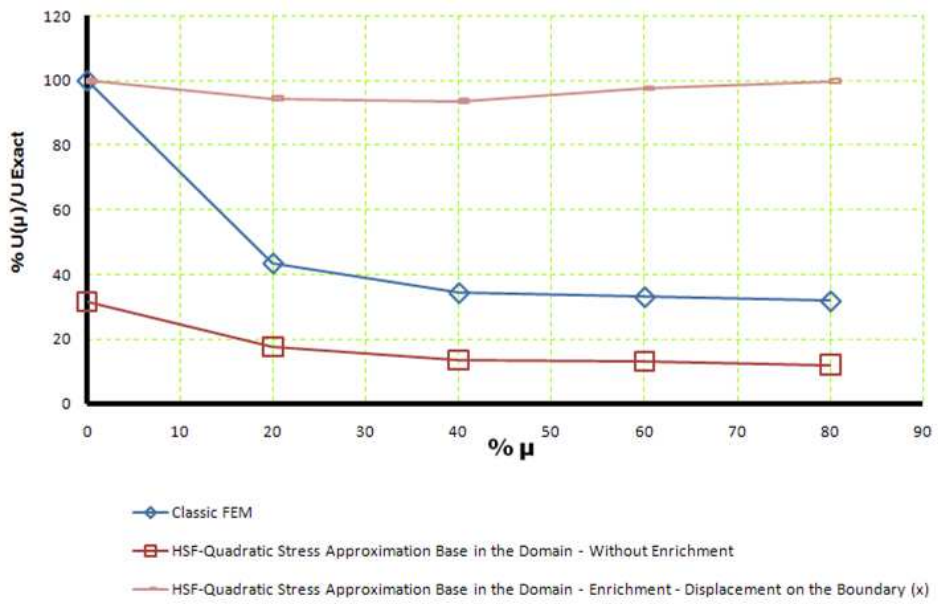
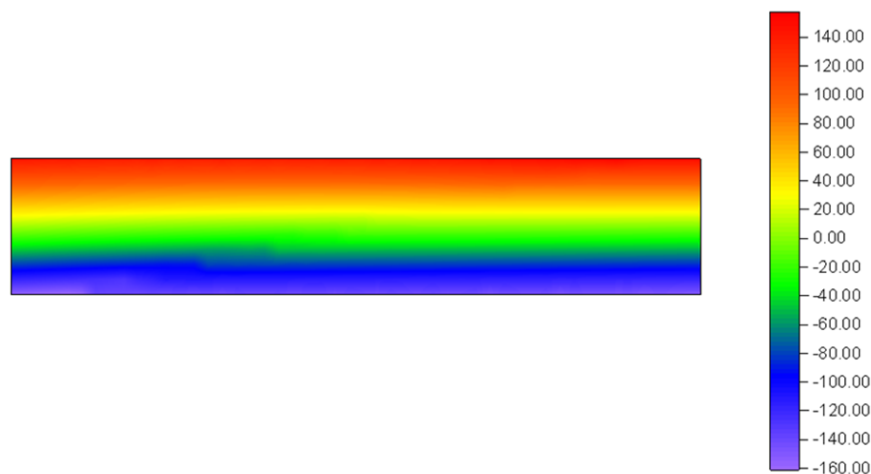


Figure 8: Strain energy - quadrilateral element mesh with nodal boundary field displacement

The effectiveness of the quadratic stress approximation combined with nodal enrichment can be verified in [Figure 9](#), where the stress distribution (σ_x) for the problem a) on a distortion condition of $\mu = 0,8$ is shown.



σ_x Quadrilateral Element ($\% \mu = 80$) \Rightarrow with enrichment

Figure 9: Stress component - σ_x - quadrilateral element mesh and nodal enrichment

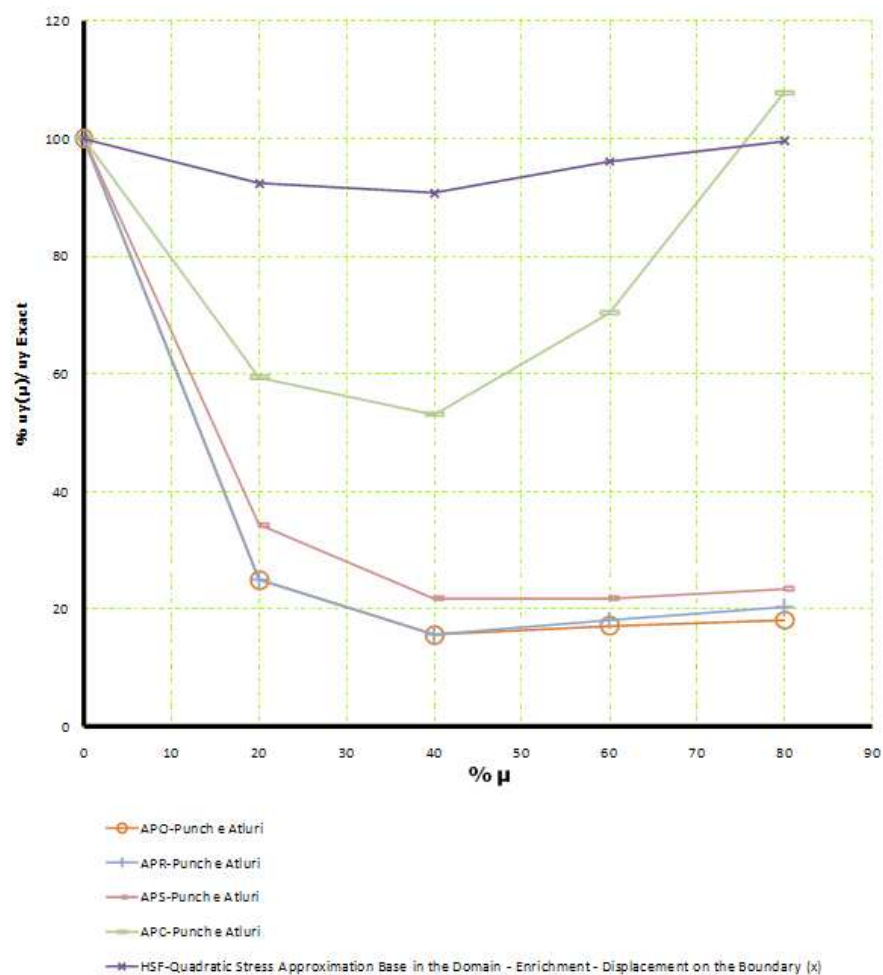


Figure 10: Comparison of normalized displacement - Punch and Atluri (1984) and GFEM-HSF

The comparison with some class of similar hybrid quadrilateral elements studied in [Punch and Atluri \(1984\)](#) indicates that they are more sensitive to mesh distortion than the HSF quadrilateral element with quadratic stress approximation and nodal enrichment, see [Figure 10](#).

In [Figure 10](#), the four-node quadrilateral elements analyzed in [Punch and Atluri \(1984\)](#) have following notation: APR: least-order a priori equilibrated Cartesian stress field in a hybrid stress functional, APO: a posteriori equilibrated cartesian stress field in a Hellinger-Reissner functional, APC: a posteriori equilibrated curvilinear stress field in a Hellinger-Reissner functional and APS: a posteriori equilibrated centroidal stress field in a Hellinger-Reissner functional.

Concerning the problem b), [Figure 11](#) illustrates that the HSF quadrilateral element without enrichment, analogously to the FEM classic element, loses efficiency when the distortion parameter increases.

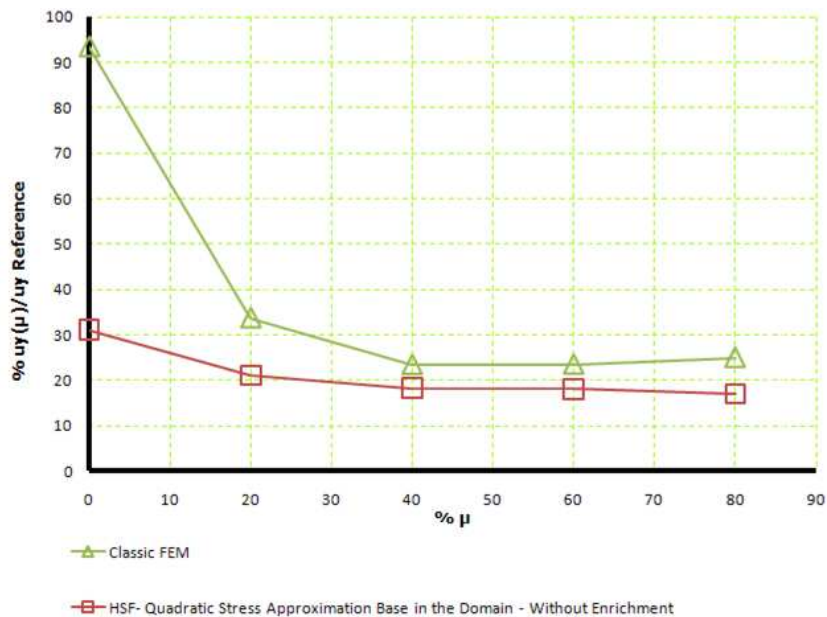


Figure 11: Normalized displacement - quadrilateral element mesh without enrichment

However, as shown in [Figure 12](#) and [Figure 13](#), the nodal enrichment improves the element robustness.

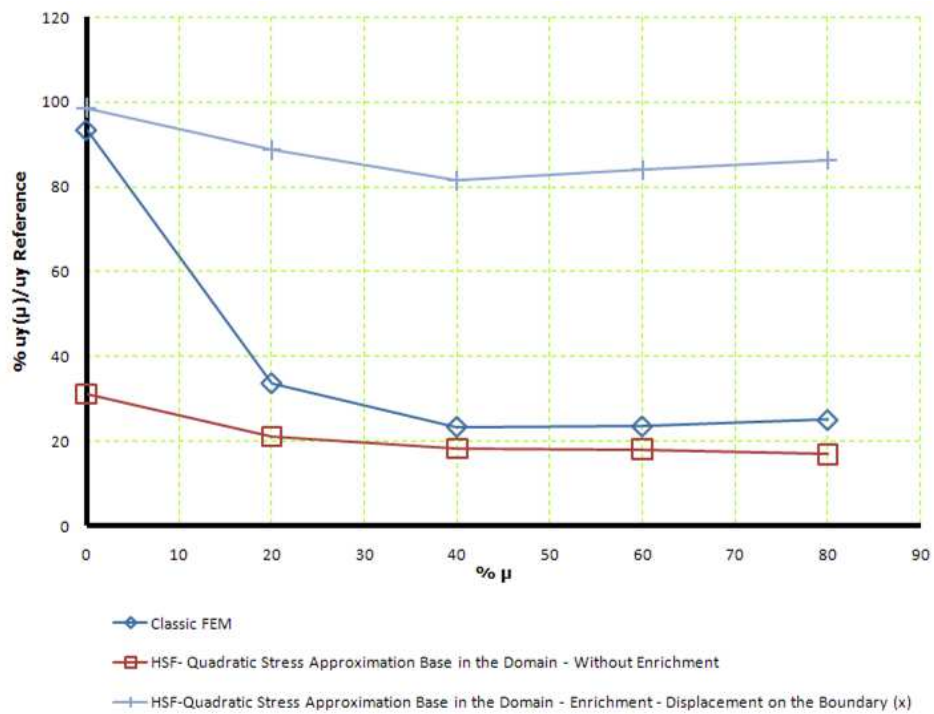


Figure 12: Normalized displacement - quadrilateral element mesh with and without nodal enrichment

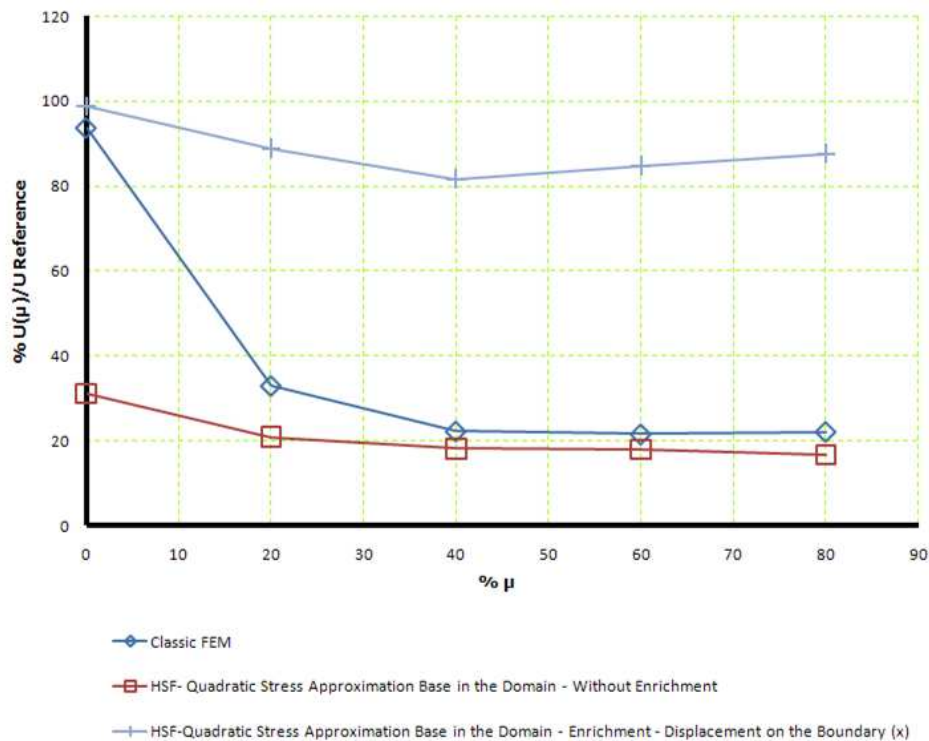


Figure 13: Strain energy - quadrilateral element mesh with and without nodal enrichment

Again, the comparison with the elements proposed by [Punch and Atluri \(1984\)](#) depicted in [Figure 14](#) highlights the performance of the proposed strategy.

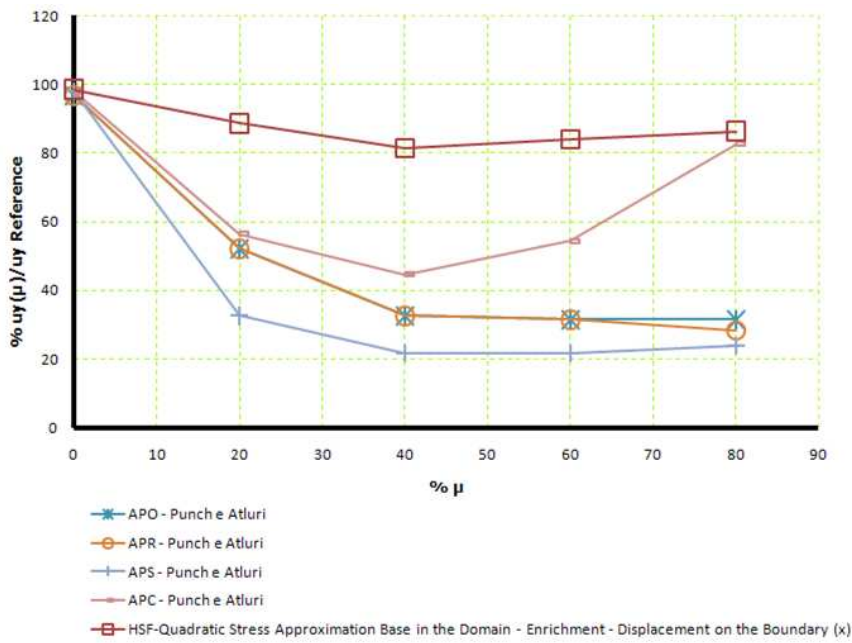


Figure 14: Comparison normalized displacement - Punch and Atluri (1984) and GFEM-HSF

The next example is a benchmark for linear plane analysis and is illustrated in [Figure 15](#). The problem was proposed by [Cook \(1987\)](#), consisting of a cantilever plate of unit thickness and submitted to a uniform distributed loading applied at its free end, as depicted in [Figure 15](#).

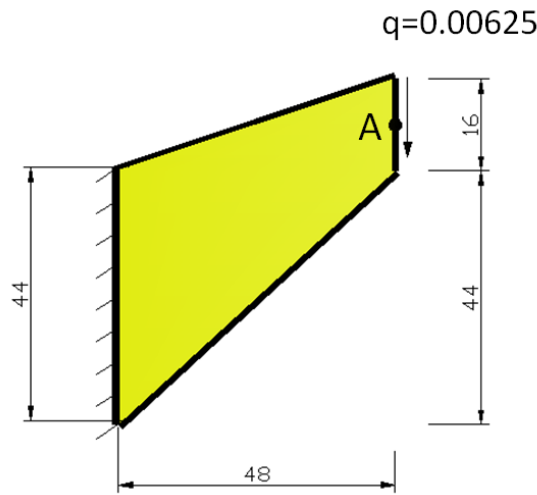


Figure 15: Cook's Panel

Assuming $E = 10$ for the Young modulus and $\nu = \frac{1}{3}$ to the Poisson's coefficient, the following reference results were obtained using an 'over killing' discretization: Strain energy: $1,20 \cdot 10^{-2}$ and vertical displacement at point A at the free boundary: $u_y = -0,239$.

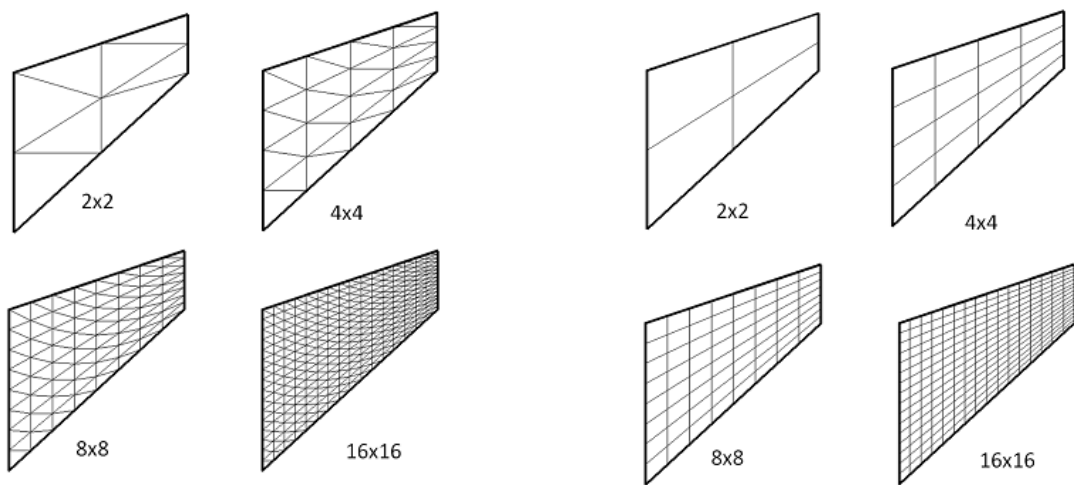


Figure 16: Triangular and quadrilateral meshes

The basic aim here is to check the convergence responses in terms of strain energy and displacement at point A (see, Figure 15). The simulations were conducted considering distorted quadrilateral and triangular element meshes, as shown in Figure 16. Analogously to the previous analysis, the enrichment was applied to the whole set of nodes except to the ones with prescribed null displacements.

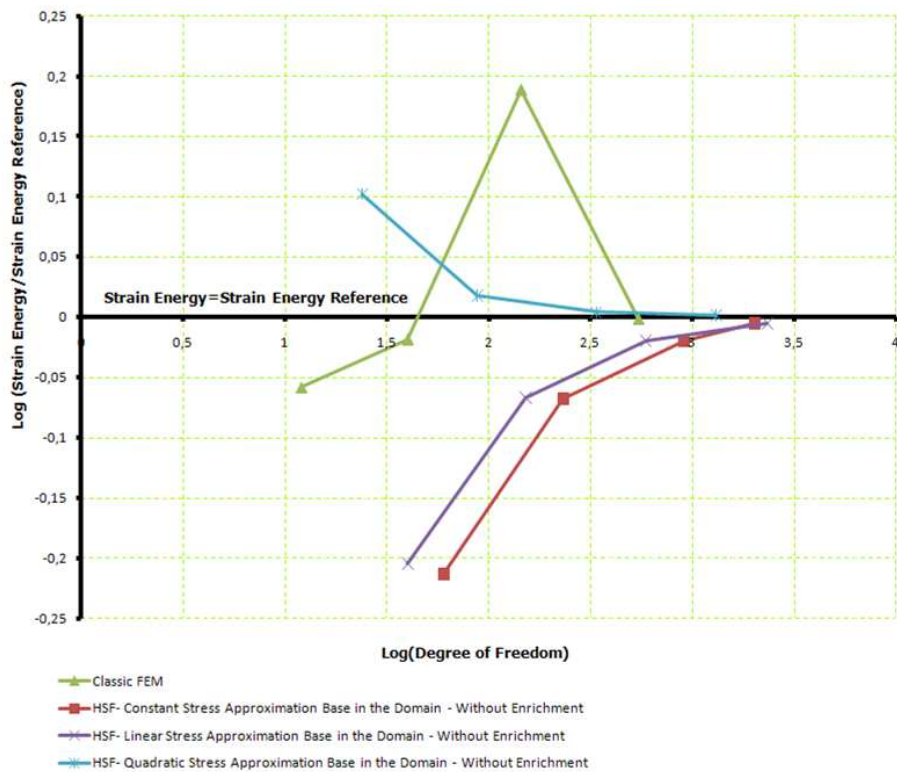


Figure 17: Strain Energy Convergence – quadrilateral element mesh without enrichment

Figure 17 shows the strain energy convergence for both the classical FEM quadrilateral element and the HSF quadrilateral element without enrichment on the boundary field, however exploring different level of stress approach. Unlike the FEM element, the HSF

quadrilateral element provides answers asymptotically convergent to the reference value of strain energy.

Stress Approximation Base	Triangular Element			Quadrilateral Element		
	Mesh	Displacement at point A	Relative Error (%)	Mesh	Displacement at point A	Relative Error (%)
Quadratic	2x2	-0.120	49.79	2x2	-0.148	38.08
	4x4	-0.183	23.43	4x4	-0.206	13.81
	8x8	-0.220	7.95	8x8	-0.229	4.18
	16x16	-0.234	2.09	16x16	-0.237	0.84
Linear	2x2	-0.120	49.79	2x2	-0.150	37.24
	4x4	-0.183	23.43	4x4	-0.206	13.81
	8x8	-0.220	7.95	8x8	-0.229	4.18
	16x16	-0.234	2.09	16x16	-0.237	0.84
Constant	2x2	-0.120	49.79	2x2	-0.303	-26.78
	4x4	-0.183	23.43	4x4	-0.248	-3.77
	8x8	-0.220	7.95	8x8	-0.242	-1.26
	16x16	-0.234	2.09	16x16	-0.240	-0.42

Table 1: Cook's Panel – HSF without enrichment - displacement at point A results.

Table 1 presents the relative error on the displacement at point A considering triangular and quadrilateral HSF element meshes without enrichment. In particular, the triangular mesh is apparently insensible to the stress approximation improvement considering its influence on the displacement value. Some similar feature is presented by the quadrilateral mesh once linear and quadratic stress approaches are adopted.

A quite interesting and known result is recovered in [Figure 18](#). The HSF triangular element without enrichment presents similar answer to the one obtained by the conventional FEM analysis for the whole set of meshes. However, a higher number of degrees of freedom were involved. This feature is known as the limitation principle for mixed formulations, [Fraeijs de Veubeke \(1965\)](#).

The nodal enrichment of the boundary displacement field improves the HSF triangular and quadrilateral elements performance as shown in [Figura 19](#) and [Figure 20](#). In particular, the results for the HSF quadrilateral element with quadratic stress approximation show that it is possible to recover the reference strain energy value, even with a coarse mesh. It is important to note that in order to guarantee the numerical results stability the enrichment was imposed only when linear and quadratic stress approximations were involved.

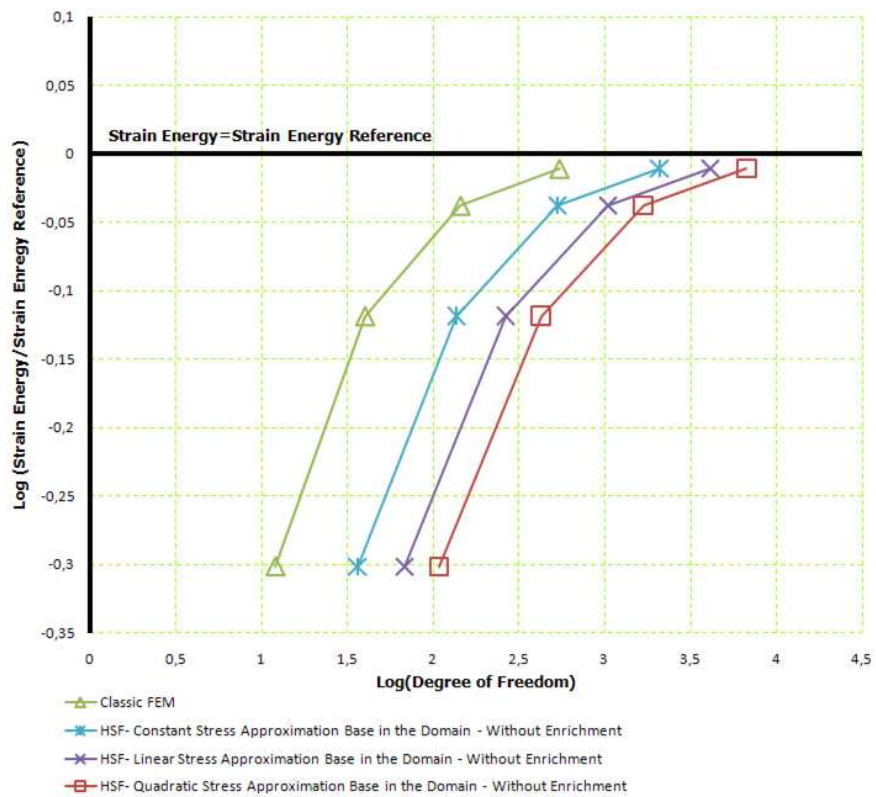


Figure 18: Strain Energy Convergence – triangular element mesh without enrichment

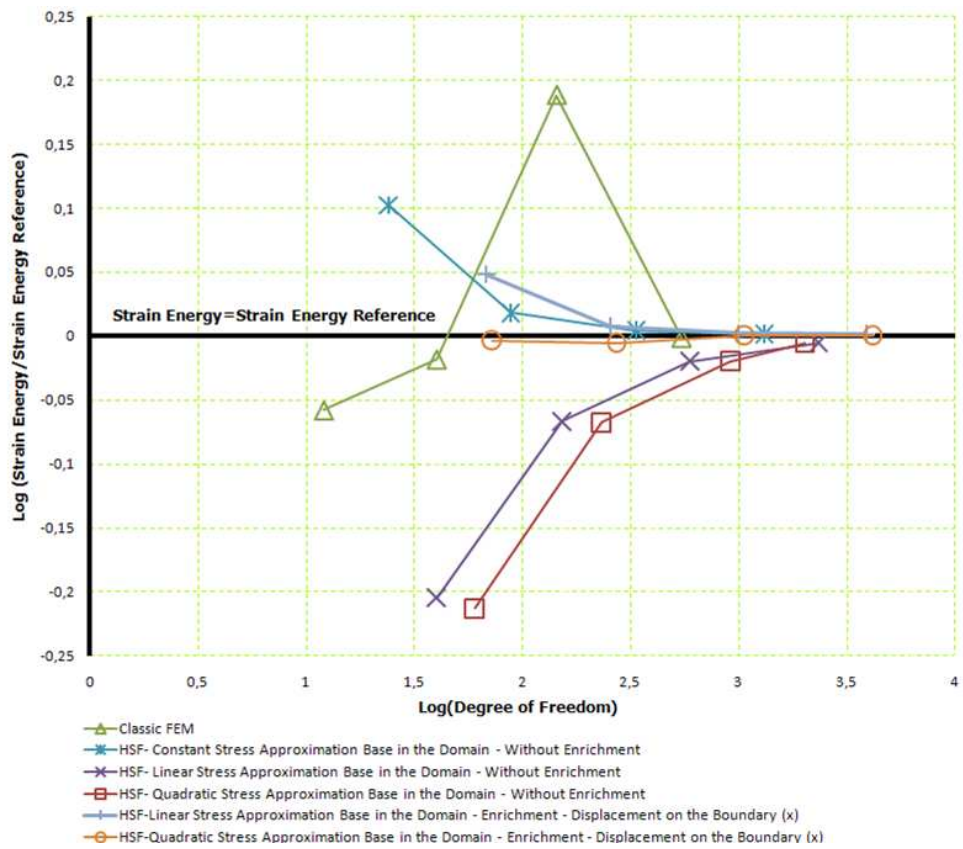


Figura 19: Strain Energy Convergence – quadrilateral element with and without nodal enrichment

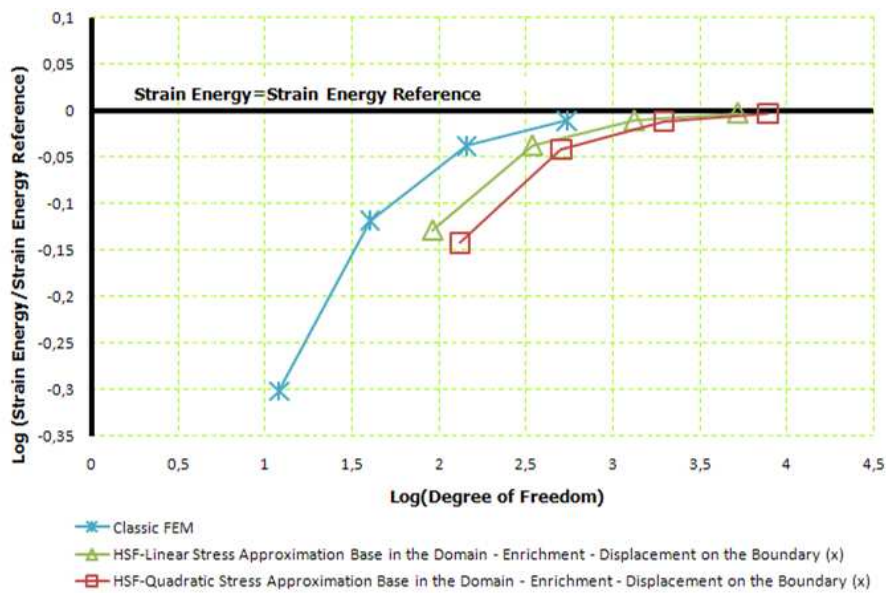


Figure 20: Strain Energy Convergence – triangular element with nodal enrichment

The effectiveness of the enrichment can also be verified considering the results listed in Table 2.

Stress Approximation Base	Triangular Element			Quadrilateral Element		
	Mesh	Displacement at point A	Relative Error (%)	Mesh	Displacement at point A	Relative Error (%)
Quadratic	2x2	-0.173	27.61	2x2	-0.239	0.01
	4x4	-0.218	8.79	4x4	-0.238	0.42
	8x8	-0.233	2.51	8x8	-0.240	-0.42
	16x16	-0.238	0.42	16x16	-0.240	-0.42
Linear	2x2	-0.179	25.10	2x2	-0.270	-12.97
	4x4	-0.220	7.95	4x4	-0.232	2.93
	8x8	-0.234	2.09	8x8	-0.240	-0.42
	16x16	-0.238	0.42	16x16	-0.240	-0.42

Table 2: Cook's Panel – HSF with nodal enrichment - displacement at point A.

5 CONCLUSIONS

The proposed numerical approach combining Hybrid Stress Formulation with nodal enrichment of the displacement boundary field, following the framework of the Generalized Finite Element, provides robust four-node quadrilateral and three-node triangular elements.

The good performance in terms of insensitivity to mesh distortion and asymptotic convergence is always effective provided the extended Zienkiewicz's inspection test is verified.

Acknowledgements

The authors would like to thank to CAPES for the granted support.

REFERENCES

- COOK, R., A plane hybrid element with rotational d.o.f and adjustable stiffness. *International Journal for Numerical Methods in Engineering*, v.24, p.1499-1508, 1987.
- Duarte, C. A., and Oden, J. T., Hp clouds – a meshless to solve boundary - value problem, The University of Texas at Austin, *Technical Report*, TICAM , 1995.
- Fraeijjs de Veubeke, B. M., Displacement and equilibrium models, in Stress Analysis, ed. by O. C. Zienkiewicz and G. Hollister, Wiley, London, 145-197, 1965; reprinted in *Int. J. Numer. Meth. Engng.*, 52, 287-342, 2001.
- Freitas, J.A.T., Almeida, J.P.B.M., and Pereira, E.M.B.R., Non-conventional formulations for the finite element method, *Structural Engineering and Mechanics* 4 , 655-678, 1996.
- Góis, W., and Proença, S. P. B. Elementos finitos híbridos com enriquecimento nodal. In: *Congresso Ibero Latino-American Sobre Métodos Computacionais em Engenharia*, 28., Porto, Portugal, Junho, 2007. Proceedings... Porto, Portugal: APMTAC, p. 1-17. 1 CD-ROM, 2007.
- Góis, W., and Proença, S. P. B., Generalized finite element method in mixed variational formulation: a study of convergence and stability. In: *Advances in Meshfree Techniques*. v.5. Heilderberg: Springer Verlag, 2007.
- Góis, W., Stress hybrid and hybrid-mixed finite elements with nodal enrichment, PhD Thesis (in Portuguese), São Carlos School of Engineering, University of São Paulo, 2009.
- Góis, W., and Proença, S.P.B., Elementos finitos híbridos e híbrido-mistas de tensão com enriquecimento nodal. *Cadernos de Engenharia de Estruturas*, v.11, n.51, ISSN: 1809-5860, 2009.
- Oden, J.T., Duarte, C.A., and Zienkiewicz, O.C., A new cloud – based hp finite element method, *Computer Methods in Applied Mechanics and Engineering*, 153, 117-126, 1998.
- Punch, E.F., and Atluri, S. N., Development and testing of stable, invariant, isoparametric curvilinear 2- and 3-d hybrid-stress elements. *Computer Methods in Applied Mechanics and Engineering*, v.47, p. 331-356, 1984.